

Iron Chemistry of a Pentadentate Ligand That Generates a Metastable Fe^{III}–OOH Intermediate

Gerard Roelfes,[†] Marcel Lubben,[†] Kui Chen,[‡] Raymond Y. N. Ho,[‡] Auke Meetsma,[†] Susan Genseberger,[§] Roel M. Hermant,[§] Ronald Hage,[§] Sanjay K. Mandal,[‡] Victor G. Young, Jr.,[‡] Yan Zang,[‡] Huub Kooijman,^{||} Anthony L. Spek,^{||} Lawrence Que, Jr.,^{*,‡} and Ben L. Feringa^{*,†}

Department of Organic and Molecular Inorganic Chemistry, University of Groningen, Nijenborgh 4, 9747 AG Groningen, The Netherlands, Department of Chemistry and Center for Metals in Biocatalysis, University of Minnesota, Minneapolis, Minnesota 55455, Unilever Research Laboratory, Olivier van Noortlaan 120, 3133 AT Vlaardingen, The Netherlands, and Crystal and Structural Chemistry, Bijvoet Center for Biomolecular Research, University of Utrecht, Padualaan 8, 3584 CH Utrecht, The Netherlands

Received August 14, 1998

In an effort to gain more insight into the factors controlling the formation of low-spin non-heme Fe^{III}–peroxo intermediates in oxidation catalysis, such as activated bleomycin, we have synthesized a series of iron complexes based on the pentadentate ligand N4Py (N4Py = *N,N*-bis(2-pyridylmethyl)-*N*-(bis-2-pyridylmethyl)amine). The following complexes have been prepared: [(N4Py)Fe^{II}(CH₃CN)](ClO₄)₂ (**1**), [(N4Py)Fe^{II}Cl](ClO₄) (**2**), [(N4Py)-Fe^{III}OMe](ClO₄)₂ (**3**), and [(N4Py)₂Fe₂O](ClO₄)₄ (**4**). Complexes **1** and **2** have low- and high-spin Fe^{II} centers, respectively, whereas **3** is an Fe^{III} complex that undergoes a temperature-dependent spin transition. The iron centers in the oxo-bridged dimer **4** are antiferromagnetically coupled ($J = -104 \text{ cm}^{-1}$). Comparison of the crystal structures of **1**, **3**, and **4** shows that the ligand is well suited to accommodate both Fe^{II} and Fe^{III} in either spin state. For the high-spin Fe^{III} complexes **3** and **4** the iron atoms are positioned somewhat outside of the cavity formed by the ligand, while in the case of the low-spin Fe^{II} complex **1** the iron atom is retained in the middle of the cavity with approximately equal bond lengths to all nitrogen atoms from the ligand. On the basis of UV/vis and EPR observations, it is shown that **1**, **3**, and **4** all react with H₂O₂ to generate the purple low-spin [(N4Py)-Fe^{III}OOH]²⁺ intermediate (**6**). In the case of **1**, titration experiments with H₂O₂ monitored by UV/vis and ¹H NMR reveal the formation of [(N4Py)Fe^{III}OH]²⁺ (**5**) and the oxo-bridged diiron(III) dimer (**4**) prior to the generation of the Fe^{III}–OOH species (**6**). Raman spectra of **6** show distinctive Raman features, particularly a $\nu(\text{O}=\text{O})$ at 790 cm⁻¹ that is the lowest observed for any iron–peroxo species. This observation may rationalize the reactivity of low-spin Fe^{III}–OOH species such as “activated bleomycin”.

Introduction

Mononuclear non-heme iron centers in enzymes play a central role in many metabolically important reactions that employ dioxygen.^{1,2} For example, Rieske and catechol dioxygenases are involved in the degradation of aromatic molecules, isopenicillin N synthase and some α -keto acid-dependent enzymes are essential for the biosynthesis of various β -lactam antibiotics,^{3,4} and lipoxygenases oxidize unsaturated fatty acids to the corresponding hydroperoxide derivatives.⁵ A particularly interesting non-heme iron requiring natural product, iron bleomycin (Fe–BLM),⁶ is a metalloglycopeptide with antitumor activity which

catalyzes oxidative DNA cleavage and oxidation of a number of organic substrates with dioxygen or H₂O₂.⁷ A common feature of the mechanisms of these systems is the involvement of an iron–peroxo species. In the case of Fe–BLM, a metastable species called “activated BLM” has been identified and is believed to be responsible for its reactivity in DNA cleavage and substrate oxidation. “Activated BLM” has been formulated by electrospray mass spectrometry as an Fe^{III}–OOH complex.^{8,9}

The best synthetic models for Fe–BLM to date are the iron complexes of the pentadentate ligands PMA¹⁰ and PYML,¹¹ which provide a very similar ligand environment around the iron center (Chart 1). Like Fe^{II}BLM, Fe^{II}PMA and Fe^{II}PYML

[†] University of Groningen.

[‡] University of Minnesota.

[§] Unilever Research Laboratory.

^{||} University of Utrecht.

(1) Que, L., Jr.; Ho, R. Y. N. *Chem. Rev.* **1996**, *96*, 2607–2624.

(2) Feig, A. L.; Lippard, S. J. *Chem. Rev.* **1994**, *94*, 759–805.

(3) Kivirikko, K. I.; Myllylä, R.; Pihlajaniemi, T. *FASEB J.* **1989**, *3*, 1609–1617.

(4) Baldwin, J. E.; Bradley, M. *Chem. Rev.* **1990**, *90*, 1079–1088.

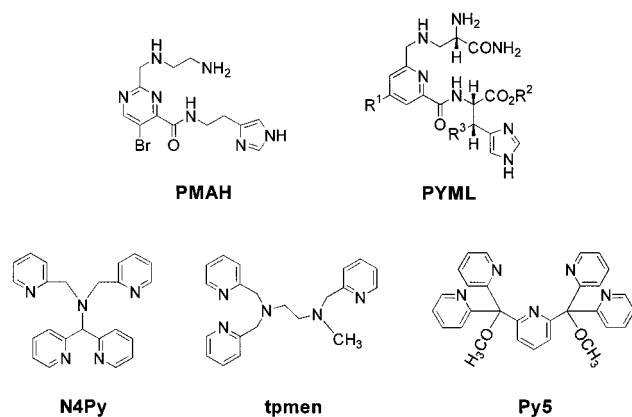
(5) Nelson, M. J.; Seitz, S. In *Active Oxygen in Biochemistry*; Valentine, J. S., Foote, C. S., Greenberg, A., Liebman, J. F., Eds.; Blackie Academic and Professional, Chapman and Hall: Glasgow, U.K., 1995; pp 276–312.

(6) Abbreviations used: acac = acetylacetonate; BLM = bleomycin; bpy = 2,2'-bipyridine; N4Py = *N,N*-bis(2-pyridylmethyl)-*N*-(bis-2-pyridylmethyl)amine; phen = 1,10-phenanthroline; TPA = tris(2-pyridylmethyl)amine; 6-Me-TPA = (6-methyl-2-pyridylmethyl)bis(2-pyridylmethyl)amine.

(7) Stubbe, J.; Kozarich, J. W.; Wu, W.; Vanderwall, D. E. *Acc. Chem. Res.* **1996**, *29*, 322–330.

(8) Sam, J. W.; Tang, X. J.; Peisach, J. *J. Am. Chem. Soc.* **1994**, *116*, 5250–5256.

(9) Marusak, R. A.; Meares, C. F. In *Active Oxygen in Biochemistry*; Valentine, J. S., Foote, C. S., Greenberg, A., Liebman, J. F., Eds.; Blackie Academic and Professional, Chapman and Hall: Glasgow, U.K., 1995; pp 342–349.

Chart 1. Pentadentate N5 Ligands That Form Metastable Fe^{III}–OOH Complexes

react with O₂ to generate low-spin iron(III) intermediates, which have EPR parameters nearly identical to those of “activated BLM”. However, there is no direct spectroscopic evidence for the Fe^{III}–OOH formulation. Such evidence has been obtained for the metastable Fe^{III}–OOH complexes of other pentadentate N5 ligands such as N4Py,^{12,13} tpmen,¹⁴ and Py5¹⁵ (Chart 1). For example, treatment of the iron(II) complex [(N4Py)Fe^{II}(CH₃CN)](ClO₄)₂ (**1**) with excess H₂O₂ in acetone affords a transient purple species ($\lambda_{\text{max}} = 530 \text{ nm}$, $\epsilon = 1100 \text{ M}^{-1} \text{ cm}^{-1}$) which exhibits EPR signals at $g = 2.17, 2.12,$ and 1.98 , resembling those of the low-spin Fe^{III} center of activated BLM. The formulation of the purple intermediate as the Fe^{III}–OOH species, [(N4Py)FeOOH]²⁺ (**6**),¹² was established using electrospray ionization mass spectroscopy with prominent peaks found at m/z 555 and 753, corresponding to the positive and negative molecular ions, {[N4Py)FeOOH](ClO₄)₃}⁺ and {[N4Py)FeOOH]-(ClO₄)₃}⁻ respectively, and their isotope distribution patterns which matched those calculated for their formulas. In this paper we report the syntheses and characterization of several Fe^{II} and Fe^{III} complexes of N4Py that serve as precursors of the [(N4Py)-FeOOH]²⁺ intermediate and summarize the spectroscopic properties of this intermediate.

Experimental Section

Syntheses. N4Py and [(N4Py)Fe(CH₃CN)](ClO₄)₂ (**1**) were prepared as previously reported.^{12,13} Commercially available chemicals were purchased and used without further purification. **CAUTION:** Perchlorate salts are potentially explosive and should be handled with care!

[(N4Py)FeCl](ClO₄)₂·H₂O (2**).** To a solution of N4Py (90 mg, 0.25 mmol) in methanol (5 mL) was added FeCl₂·4H₂O (50 mg, 0.25 mmol). After stirring for 2 h, NaClO₄ (32.5 mg, 0.27 mmol) was added, and the solution was then stirred for an additional 15 min. After filtration, the filtrate was placed in an ether bath to yield orange crystals of **2**

(118 mg, 86%) overnight. ¹H NMR (ppm, acetone-*d*₆): $\delta -1.8, 29.7, 30.2, 40.6, 52.1, 52.9, 56.5, 91, 116, 141, 161$. Anal. Calcd for C₂₃H₂₃Cl₂FeN₅O₅: C, 47.94; H, 4.02; N, 12.15. Found: C, 47.63; H, 3.99; N, 11.88.

[(N4Py)FeOMe](ClO₄)₂·H₂O (3**). Method A.** To a solution of N4Py (430 mg, 1.17 mmol) in methanol (4 mL) was added a solution of Fe(ClO₄)₃·xH₂O (460 mg, 1.30 mmol) in methanol (2 mL). The resulting red brown solution was stirred for 2 h at room temperature, during which time a yellow solid precipitated. The precipitate was filtered and suspended in methanol (15 mL). After heating under reflux for 1 h, the hot solution was filtered and the filtrate was heated under reflux for an additional 15 min. Upon cooling to room temperature, **3** crystallized as red plates (218 mg, 29%). UV/vis (MeOH): $\lambda_{\text{max}} 255 \text{ nm}$ ($\epsilon = 18\,000 \text{ M}^{-1} \text{ cm}^{-1}$), 360 nm ($\epsilon = 4000 \text{ M}^{-1} \text{ cm}^{-1}$). ¹H NMR (ppm, CD₃CN): $\delta -14, -1, 83, 119$. Anal. Calcd for C₂₄H₂₆Cl₂FeN₅O₁₀: C, 42.94; H, 3.90; N, 10.43. Found: C, 42.79; H, 3.86; N, 10.27.

Method B. Crystals of complex **3** were also obtained unexpectedly in an attempt to synthesize [(N4Py)Fe(acac)](ClO₄)₂ as follows. N4Py·4HClO₄ (1.43 g, 1.87 mmol) was treated with excess 1.8 M NaOH aqueous solution, which was followed by extraction with CH₂Cl₂ to give the free amine of N4Py. Sequential addition of Fe(ClO₄)₃·10H₂O (0.99 g, 1.86 mmol), acetylacetone (0.19 mL, 1.87 mmol), and triethylamine (0.26 mL, 1.87 mmol) into a methanol solution of N4Py resulted in a dark red solution. Upon standing at 4 °C, the solution yielded a yellow solid. Red crystals (**3**)₂·1.5CH₃OH suitable for X-ray analysis (refinement on *F*² with SHELXL97) were grown by slow vapor diffusion of methanol into an acetone solution of the yellow solid inside the refrigerator.

[(N4Py)₂Fe₂O](ClO₄)₄·(H₂O) (4**).** A solution of **3** (230 mg, 0.35 mmol) in CH₃CN (9 mL) was divided into 8 equal portions. These portions were placed in an ethyl acetate bath, and after 4 days **4** (161 mg, 73%) was obtained as brown crystals. UV/vis (CH₃CN): $\lambda_{\text{max}} 254 \text{ nm}$ ($\epsilon = 41\,000 \text{ M}^{-1} \text{ cm}^{-1}$), 316 nm ($\epsilon = 14\,000 \text{ M}^{-1} \text{ cm}^{-1}$). ¹H NMR (ppm, CD₃CN): $\delta 6.7, 8.1, 10, 16.7, 20.3, 25, 31$. Anal. Calcd for C₄₆H₄₂Cl₄Fe₂N₁₀O₁₈: C, 43.22; H, 3.47; N, 10.96. Found: C, 42.96; H, 3.31; N, 10.98. For crystallographic studies, the complex was recrystallized by slow vapor diffusion of ethyl acetate into an CH₃CN solution of **4** to afford the tris-acetonitrile solvate.

Physical Methods. ¹H NMR spectra were recorded on a Varian Gemini 300 spectrometer at ambient temperature. Chemical shifts (in ppm) were referenced to the residual protic solvent peaks. EPR spectra were obtained at liquid nitrogen temperature on a Bruker ECS106 instrument or at liquid helium temperatures on a Bruker E500 equipped with an Oxford Instruments ESR-10 cryostat. Visible spectra were recorded on a Hewlett-Packard 8453 diode array spectrophotometer. Electrochemical studies were carried out with a PAR 273A potentiostat in acetonitrile using 0.1 M tetrabutylammonium perchlorate as the supporting electrolyte. Cyclic voltammograms (CV) were obtained by using a three-component system consisting of a glassy carbon working electrode, a platinum wire auxiliary electrode, and a saturated calomel reference electrode. Variable temperature magnetic susceptibility data were collected on a Quantum Design SQUID susceptometer; the diamagnetic corrections for the complexes were calculated using Pascal’s constants¹⁶ and subtracted from the data prior to fitting the data. Resonance Raman samples of **6** were prepared by adding 50 mM H₂O₂ to a 10 mM [Fe^{II}(N4Py)(CH₃CN)]²⁺ solution in *d*₆-acetone at -10 °C. The spectra were collected on an Acton AM-506 spectrometer (2400-groove grating) using a Kaiser Optical holographic super-notch filter with a Princeton Instruments liquid N₂ cooled (LN-1100PB) CCD detector with 4 cm⁻¹ spectral resolution. Spectra were obtained with a backscattering geometry on liquid N₂ frozen samples using 615 nm laser excitation from a 375B CW dye (Rhodamine 6G) laser pumped by a Spectra Physics 2030-15 argon ion laser. Raman frequencies were referenced to indene. For the labeling studies, H₂¹⁸O₂ (90% ¹⁸O, ICON Services Inc.) and acetone or H₂O₂ diluted in D₂O was used.

Crystallographic Studies. Crystals of the complexes **1** and **4** were glued to the tip of a glass fiber and cooled to 130 K by using an online

- (10) (a) Guajardo, R. J.; Hudson, S. E.; Brown, S. J.; Mascharak, P. K. *J. Am. Chem. Soc.* **1993**, *115*, 7971–7977. (b) Guajardo, R. J.; Chavez, F.; Farinas, E. T.; Mascharak, P. K. *J. Am. Chem. Soc.* **1995**, *117*, 3883–3884.
- (11) (a) Kittaka, A.; Sugano, Y.; Otsuka, M.; Ohno, M.; Sugiura, Y.; Umezawa, H. *Tetrahedron Lett.* **1986**, *27*, 3631–3634. (b) Sugano, Y.; Kittaka, A.; Otsuka, M.; Ohno, M.; Sugiura, Y.; Umezawa, H. *Tetrahedron Lett.* **1986**, *27*, 3635–3638.
- (12) Lubben, M.; Meetsma, A.; Wilkinson, E. C.; Feringa, B.; Que, L., Jr. *Angew. Chem., Int. Ed. Engl.* **1995**, *34*, 1512–1514.
- (13) Roelfes, G.; Lubben, M.; Leppard, S. W.; Schudde, E. P.; Hermant, R. M.; Hage, R.; Wilkinson, E. C.; Que, L., Jr.; Feringa, B. L. *J. Mol. Catal., A* **1997**, *117*, 223–227.
- (14) Bernal, I.; Jensen, I. M.; Jensen, K. B.; McKenzie, C. J.; Toftlund, H.; Tuchagues, J. P. *J. Chem. Soc., Dalton Trans.* **1995**, 3667–3675.
- (15) de Vries, M. E.; La Crois, R. M.; Roelfes, G.; Kooijman, H.; Spek, A. L.; Hage, R.; Feringa, B. L. *J. Chem. Soc., Chem. Commun.* **1997**, 1549–1550.

- (16) Boudreaux, E. A.; Mulay, L. N. *Theory and Applications of Molecular Paramagnetism*; John Wiley and Sons: New York, 1976.

Table 1. Crystallographic Data

	1	3	4
empirical formula	C ₂₆ H ₂₈ Cl ₂ FeN ₆ O ₉	C _{49.5} H ₅₄ Cl ₄ Fe ₂ N ₁₀ O _{19.5}	C ₅₂ H ₅₁ Cl ₄ Fe ₂ N ₁₃ O ₁₇
fw (g mol ⁻¹)	695.30	1354.53	1383.56
cryst syst	monoclinic	orthorhombic	monoclinic
space group	<i>P2₁/n</i>	<i>Pbca</i>	<i>I2/m</i>
<i>a</i> (Å)	12.191(1)	21.3348(1)	11.730(1)
<i>b</i> (Å)	18.500(1)	16.6471(1)	18.640(2)
<i>c</i> (Å)	13.015(1)	32.1048(4)	13.331(2)
β (deg)	95.928(8)		93.74(2)
<i>V</i> (Å ³)	2919.6(4)	11402.4(2)	2908.6(6)
<i>Z</i>	4	8	2
<i>D</i> _{calc} (g cm ⁻³)	1.582	1.578	1.580
<i>T</i> (K)	130	173	130
λ (Å)	0.710 73	0.710 73	0.710 73
μ (cm ⁻¹)	7.6	7.81	7.65
<i>R</i> _F ^a	0.046		0.063
<i>R</i> _I ^b		0.070	
<i>R</i> _w ^c	0.049		0.061
<i>wR</i> ₂ ^d		0.115	

$$^a R_F = \sum(|F_o| - |F_c|) / \sum|F_o|. \quad ^b R_I = \sum||F_o| - |F_c|| / \sum|F_o|. \quad ^c R_w = [\sum(w(|F_o| - |F_c|)^2) / \sum w|F_o|^2]^{1/2}. \quad ^d wR_2 = [\sum[w(F_o^2 - F_c^2)^2] / \sum[w(F_o^2)^2]]^{1/2}.$$

liquid nitrogen cooling system mounted on an Enraf-Nonius CAD-4F diffractometer interfaced to a MicroVAX-2000 computer. Unit cell parameters and orientation matrices were determined from a least-squares refinement by using the setting angles of 22 well-centered reflections. The standard reflections were measured every 3 h of X-ray exposure time as a check for crystal deterioration and/or misalignment. Intensity data were corrected for Lorentz and polarization effects and scale variation, but not for absorption. Pertinent crystallographic data and experimental conditions are summarized in Table 1. The structures were solved by Patterson methods, and extension of the model was accomplished by direct methods applied to difference structure factors using the program DIRDIF. The positional and anisotropic thermal displacement parameters for the non-hydrogen atoms were refined with block-diagonal least-squares procedures. A subsequent difference Fourier synthesis resulted in the location of all hydrogen atoms. Refinement was carried out with full-matrix least squares on *F_o* by full-matrix least-squares techniques with anisotropic thermal displacement parameters for the non-hydrogen atoms and isotropic thermal displacement parameters for the hydrogen atoms.

X-ray diffraction studies of (3)₂·1.5CH₃OH with dimensions of 0.26 × 0.21 × 0.07 mm were performed on a Siemens SMART Platform CCD system with graphite-monochromated Mo K α radiation (λ = 0.710 73 Å). Data were collected at 173(2) K with θ values ranging from 1.27° to 25.04°. The structure was solved by direct methods and full-matrix least-squares/difference Fourier cycles. Hydrogen atoms were treated as idealized distributions.

Results and Discussion

Synthesis and Characterization of Iron Complexes of N4Py. As previously described, the pentadentate ligand N4Py reacts with either Fe(ClO₄)₃ or Fe(ClO₄)₂ in methanol/acetonitrile mixtures to give a red crystalline complex **1** formulated as [(N4Py)Fe(CH₃CN)](ClO₄)₂.^{12,13} Complex **1** is EPR-silent and exhibits a ¹H NMR spectrum with peaks only in the diamagnetic region, consistent with **1** being a low-spin Fe^{II} complex. The fact that the Fe^{II} complex was obtained no matter whether Fe(ClO₄)₃ or Fe(ClO₄)₂ was used can be rationalized by the high potential of **1** (1.01 V vs SCE) for the Fe^{III}/Fe^{II} couple in acetonitrile.

In contrast, complexation of N4Py with FeCl₂ in methanol in the presence of NaClO₄ yielded an orange crystalline complex **2**, characterized as [(N4Py)FeCl](ClO₄). In this case, its ¹H NMR spectrum in acetone-*d*₆ has relatively sharp paramagnetically shifted signals in the -2 to 160 ppm range, indicative of a high-spin Fe^{II} complex. Cyclic voltammetry of **2** in acetonitrile shows a reversible wave at 590 mV vs SCE ascribed to the Fe^{III}/Fe^{II} couple. The lower oxidation potential of **2** compared

to that of **1** reflects the replacement of the neutral CH₃CN ligand in **1** with an anionic Cl⁻ ligand in **2**, giving rise to a high-spin Fe^{II} complex.

Reaction of N4Py with Fe(ClO₄)₃·xH₂O in methanol (in the absence of acetonitrile) afforded a yellow precipitate containing both mononuclear Fe^{III} and oxo-bridged dinuclear Fe^{III} species as judged by ¹H NMR spectroscopy. Recrystallization of this mixture from hot methanol resulted in a red crystalline compound which was characterized as an Fe^{III}-methoxy complex, [(N4Py)FeOMe](ClO₄)₂ (**3**). The ¹H NMR spectrum of **3** shows broad paramagnetically shifted signals at -10 to 0 ppm and 80 to 120 ppm, characteristic of high-spin Fe^{III}-pyridine complexes.^{17,18} However, the EPR spectrum of **3** at 4 K in frozen methanol shows one signal at *g* ~ 6, associated with an axial *S* = 5/2 complex, and a second set of signals at *g* = 2.29, 2.12, and 1.96 which is characteristic of an *S* = 1/2 complex. This result is inconsistent with the ¹H NMR spectrum at room temperature and suggests a temperature-dependent spin transition. Variable-temperature magnetic susceptibility experiments support this notion. The μ_{eff} of complex **3** is found to be 5.8 μ_B at room temperature, but decreases to a constant value of 4.0 μ_B at 70–10 K (Figure 1). A detailed analysis of this behavior cannot be provided at present, but the following picture is consistent with the available information. The high-spin form of **3** is favored at high temperature affording the μ_{eff} value expected for an *S* = 5/2 system. As the temperature is lowered, one of the two cations in the asymmetric unit (**3b**, see next section) converts to a low-spin form. Thus at 70 K, half of the complexes are *S* = 5/2 and the other half are *S* = 1/2. Such a mixture would be expected to have a μ_{eff} value of about 4.4 μ_B . Taken together, the spin state of the Fe^{III} center of complex **3** is temperature-dependent with the low-spin state favored at low temperature.

Dissolving **3** in acetonitrile followed by slow vapor diffusion of ethyl acetate into this solution resulted in the formation of a brown crystalline complex, characterized as [(N4Py)₂Fe₂O](ClO₄)₄ (**4**), in 73% yield. The ¹H NMR spectrum of **4** displays signals in the 0–40 ppm range, as found for antiferromagnetically coupled (μ -oxo)diiron(III) TPA complexes.¹⁹ The variable-

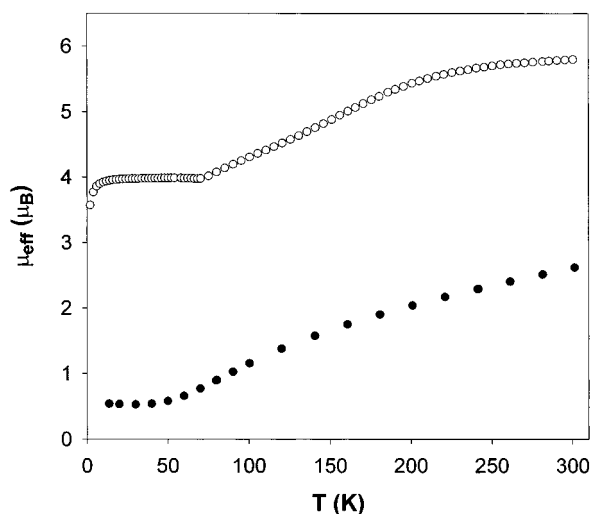
(17) Jang, H. G.; Cox, D. D.; Que, L., Jr. *J. Am. Chem. Soc.* **1991**, *113*, 9200–9204.

(18) Zang, Y.; Kim, J.; Dong, Y.; Wilkinson, E. C.; Appelman, E. H.; Que, L., Jr. *J. Am. Chem. Soc.* **1997**, *119*, 4197–4205.

(19) Norman, R. E.; Holz, R. C.; Ménage, S.; O'Connor, C. J.; Zhang, J. H.; Que, L., Jr. *Inorg. Chem.* **1990**, *29*, 4629–4637.

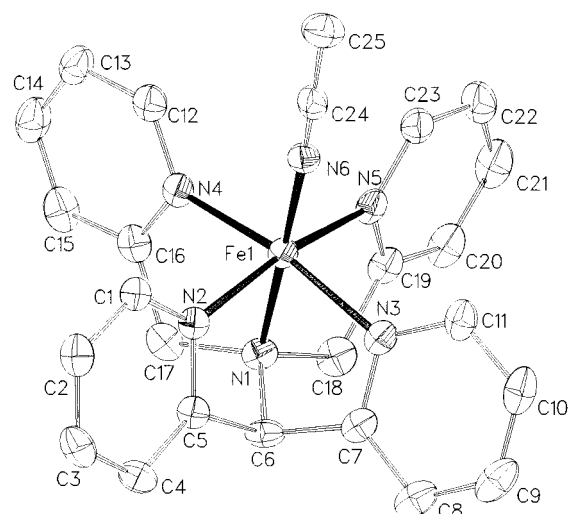
Table 2. Selected Bond Distances and Bond Angles for [(N4Py)Fe(CH₃CN)]²⁺ (**1**), [(N4Py)FeOMe]²⁺ (**3**), and [(N4Py)₂Fe₂O]⁴⁺ (**4**)^a

	1		3a		3b		4	
Fe–N _{amine} (Å)	(N1)	1.961(3)	(N1)	2.198(3)	(N6)	2.100(3)	(N3)	2.244(5)
Fe–N _{py} (Å)	(N2)	1.976(3)	(N3)	2.114(3)	(N8)	2.047(4)	(N2)	2.144(4)
	(N3)	1.967(3)	(N2)	2.138(3)	(N7)	2.073(3)		
	(N4)	1.968(3)	(N4)	2.105(3)	(N9)	2.040(4)	(N1)	2.107(4)
	(N5)	1.975(3)	(N5)	2.094(3)	(N10)	2.024(4)		
Fe–N _{acetonitrile} (Å)	(N6)	1.915(3)						
Fe–N _{py} -mean plane (Å)		0.2071(5)		0.463(2)		0.352(2)		0.5307(9)
Fe–O (Å)			(O1)	1.772(3)	(O2)	1.789(3)	(O1)	1.8034(10)
Fe–O–CH ₃ (deg)				171.5(3)		136.5(5)		
Fe1–O1–Fe2 (deg)								180

^a Standard deviations are in parentheses.**Figure 1.** Temperature dependence of the magnetic moments of **3** (○) and **4** (●).

temperature magnetic susceptibility data for **4** can be fitted to the Hamiltonian $H = 2J\mathbf{S}_1 \cdot \mathbf{S}_2$ with an antiferromagnetic coupling constant of -104 cm^{-1} (Figure 1). The complex is EPR-silent, as expected for antiferromagnetically coupled Fe^{III} dimers. However, addition of MeOH affords the characteristic EPR signals of **3**. Addition of water to **4**, on the other hand, gives rise to a second set of low-spin Fe^{III} EPR signals at $g = 2.41, 2.15,$ and 1.92 , similar to those observed for (BLM)Fe^{III}–OH ($2.43, 2.14, 1.89$),²⁰ suggesting that these new signals result from [(N4Py)FeOH]²⁺ (**5**). Addition of H₂O to **3** also gives rise to these signals. These observations demonstrate that the oxo bridge of **4** is quite labile and easily broken by addition of water or methanol to give mononuclear complexes.

Crystal Structures of 1, 3, and 4. The crystal structures of **1**, **3**, and **4** were solved, and their metric parameters are compared in Table 2. The structure of the cation of **1** (Figure 2) shows a six-coordinate Fe^{II} center with five coordination sites occupied by the N atoms of the N4Py ligand. The sixth coordination site is occupied by an acetonitrile molecule, which was the solvent for crystallization. All five Fe–N bonds from the N4Py ligand are nearly equal in length at $1.97(1) \text{ Å}$. These bond length values are comparable to those found for other low-spin Fe^{II} complexes such as [(phen)₃Fe]²⁺,²¹ [(bpy)₃Fe]²⁺,²² and [(TPA)Fe(CH₃CN)₂]²⁺.¹⁸ The iron atom lies $0.2071(5) \text{ Å}$ above

**Figure 2.** ORTEP plot of [(N4Py)Fe(CH₃CN)]²⁺ (**1**). Hydrogen atoms omitted for clarity.

the mean plane formed by the four pyridine nitrogen atoms with the pyridine rings positioned perpendicular to this plane.

The crystal structure of **4** (Figure 3a) shows a complex with an inversion center at the oxo bridge. The Fe–O–Fe unit is linear, and there is a plane of symmetry through C11–N3–Fe1–O1, as illustrated by a view along the Fe–O–Fe axis in Figure 3b. Each iron center is in a distorted octahedral environment ligated by the four pyridine nitrogen atoms and the amine nitrogen, as well as the oxygen which is bound to the second iron center. The Fe–O bond length of $1.8034(10) \text{ Å}$ is as expected for an oxo bridge.²³ The Fe–N_{py} bonds of $2.107(4)$ and $2.144(4) \text{ Å}$ are comparable to those found for (μ -oxo)diiron(III) TPA complexes^{19,24} and are considerably shorter than the Fe–N_{amine} bond ($2.244(5) \text{ Å}$) which is trans to the oxo bridge. This difference in bond lengths between the Fe–N_{py} and the Fe–N_{amine} bonds has also been observed in Fe^{III}–TPA complexes.^{19,25} Again the iron center is situated above the mean plane formed by the four pyridine nitrogen atoms, with a distance of $0.5307(9) \text{ Å}$ from that plane. As shown in Figure 3b, the presence of the four pyridine rings on each iron results in a rather crowded structure. In response, the two halves of the complex are twisted from each other to relieve the steric interaction around the Fe–O–Fe bond. Such steric hindrance may rationalize the facile cleavage of the oxo bridge with proton sources as weak as H₂O and MeOH.

(20) (a) Burger, R. M.; Peisach, J.; Horwitz, S. B. *J. Biol. Chem.* **1981**, *256*, 11636–11644. (b) Sugiura, Y. *J. Am. Chem. Soc.* **1980**, *102*, 5208–5215.

(21) Zalkin, A.; Templeton, D. H.; Ueki, T. *Inorg. Chem.* **1973**, *12*, 1641–1646.

(22) Posse, G. M. E.; Juri, M. A.; Aymonino, P. J.; Piro, O. E.; Negri, H. A.; Castellano, E. E. *Inorg. Chem.* **1984**, *23*, 948–952.

(23) Kurtz, D. M., Jr. *Chem. Rev.* **1990**, *90*, 585–606.

(24) Kojima, T.; Leising, R. A.; Yan, S.; Que, L., Jr.; *J. Am. Chem. Soc.* **1993**, *115*, 11382–11335.

(25) Norman, R. E.; Yan, S.; Que, L., Jr.; Backes, G.; Ling, J.; Sanders-Loehr, J.; Zhang, J. H.; O'Connor, C. J. *J. Am. Chem. Soc.* **1990**, *112*, 1554–1562.

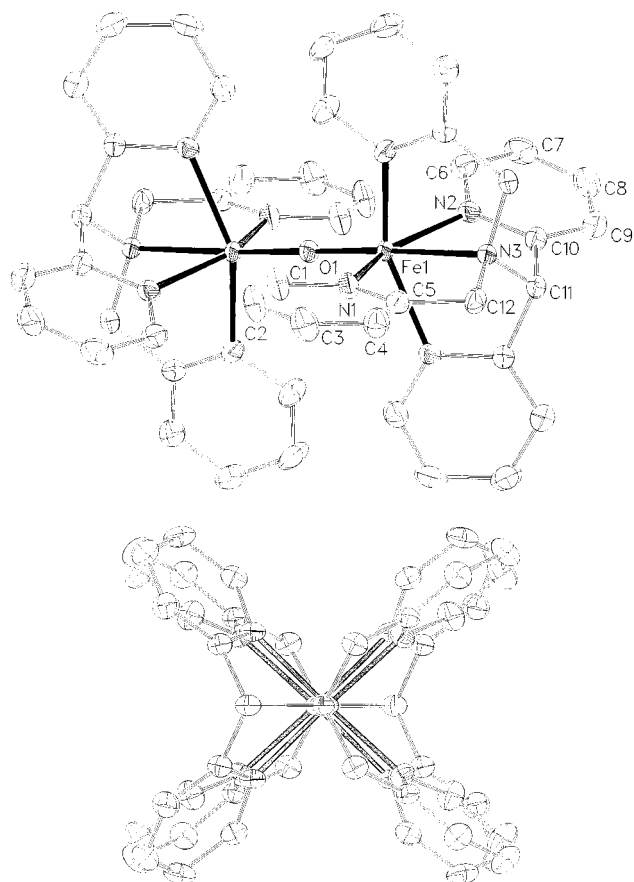


Figure 3. (a) ORTEP plot of $[(\text{N4Py})_2\text{Fe}_2\text{O}]^{4+}$ (**4**). (b) View along the Fe1–O–Fe2 axis. Hydrogen atoms omitted for clarity.

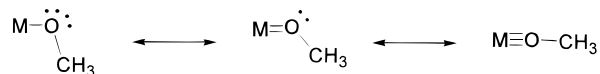
The structure of $(\mathbf{3})_2 \cdot 1.5\text{CH}_3\text{OH}$ consists of two distinct $[(\text{N4Py})\text{FeO}(\text{Me})]^{2+}$ cations in the asymmetric unit (Figure 4).²⁶ In each of the cations, the iron center is in a distorted octahedral geometry with coordination to all five nitrogen atoms of the N4Py ligand and the oxygen from the methoxy group which is trans to the amine nitrogen. However, cation **3a** has a nearly linear Fe–O–CH₃ moiety (171.5(3)°), while cation **3b** has a bent Fe–O–CH₃ moiety (136.5(5)°). The Fe–OCH₃ and O–CH₃ bonds of **3a** and **3b** also reflect this difference; **3a** has the shorter Fe–O bond (1.772(3) Å) and the longer C–O bond (1.418(6) Å), while **3b** has corresponding bond lengths of 1.789(3) and 1.375(6) Å. In addition, the stronger Fe–O bond of **3a** pulls the iron center slightly more out of the mean plane of the four pyridyl nitrogen atoms (0.463(2) Å for **3a** vs 0.352(2) Å for **3b**). Consequently, the more tightly bound methoxy group in **3a** gives rise to longer Fe–N distances with the ligated nitrogen atoms of N4Py, Fe–N_{amine} = 2.198(3) Å and average Fe–N_{py} = 2.11(2) Å, relative to 2.100(3) and 2.05(2) Å, respectively, for **3b** with the more weakly bound methoxy group. The average Fe–N_{py} bond lengths for **3a** are in the range of those found for high-spin (TPA)Fe^{III} complexes such as $[(6\text{-Me-TPA})\text{Fe}(\text{acac})]^{2+}$ (2.13(5) Å),¹⁸ and $[(\text{TPA})\text{FeCl}_2]^{+}$

(26) Crystals suitable for a single-crystal X-ray structure determination of **3** were originally obtained using method A. The resulting crystal structure is essentially equivalent to the one based on crystals obtained via method B. The main difference between both structures is the extent of conformational disorder of the alkoxy moiety. The method A type structure was refined with a 79% stretched + 21% bent Fe–O–C disorder model for one of the two independent cations and 21:79 disorder model for the other cation (Note: Bent forms on each cation cannot coexist for spatial reasons). The method B type structure shows similar disorder but barely above the noise level (i.e., highest peak in the final difference map 0.61 e/Å) and therefore not modeled.

(2.15(4) Å).²⁴ The Fe–N_{py} bond lengths for **3b** are shorter, but still considerably longer than those found for low-spin Fe^{III} complexes such as $[(5\text{-Me}_3\text{-TPA})\text{Fe}(\text{acac})]^{2+}$ (1.95(3) Å on average).¹⁸ Thus **3b** appears to have bond lengths intermediate between those typically found for low-spin Fe^{III} and high-spin Fe^{III} complexes, consistent with the spin crossover behavior of **3** discussed in the previous section.

The two $[(\text{N4Py})\text{FeO}(\text{Me})]^{2+}$ cations in the crystal structure of $(\mathbf{3})_2 \cdot 1.5\text{CH}_3\text{OH}$ represent two types of Fe^{III}-terminal alkoxy complexes (Table 3).^{27–33} As commonly found for most structurally characterized Fe^{III}-terminal alkoxy complexes, the bent Fe–O–CH₃ angle and the longer Fe–O bond in **3b** are characteristic of a singly bonded metal–alkoxy bond. On the other hand, the nearly linear Fe–O–CH₃ moiety and the shorter Fe–O bond in **3a** can be understood by considering the resonance structures proposed for electron-deficient metals such as Ti^{IV} and Zr^{IV} (Scheme 1),^{34,35} indicating more π -bonding character in the Fe^{III}–OCH₃ bond. A similarly open Fe–O–CH₃ moiety (164.9°) has also been observed in $[(\text{PY5})\text{FeO}(\text{Me})-(\text{OTf})_2]$,²⁷ and these two cases constitute a novel family of Fe^{III}-terminal alkoxy complexes in which the extremely Lewis acidic metal center may be generated from the ligation of the neutral ligands such as N4Py and PY5, as proposed by Jonas and Stack.²⁷

Scheme 1. Proposed Resonance Structures for Electron-Deficient Metal-Terminal Alkoxy Complexes



From comparison of the structures of **1**, **3**, and **4** it is clear that the N4Py ligand can accommodate both Fe^{II} and Fe^{III} ions in either a high-spin or a low-spin state very well. In the structure of **1** the iron atom is positioned in the middle of the cavity formed by the ligand, with nearly equal Fe–N bond lengths to all nitrogen atoms of the ligand. This contrasts with the Fe^{III} complexes **3** and **4**, where the iron atom lies above the ligand cavity, resulting in a longer Fe–N_{amine} bond length compared to the Fe–N_{py} bonds. This is also evident from the larger distance of the iron center from the mean plane formed by the pyridyl nitrogen atoms (0.2071, 0.4635, 0.3518, and 0.5307 Å, respectively for **1**, **3a**, **3b**, and **4**). The ease of accommodating a low-spin Fe^{II} center in the N4Py ligand cavity could rationalize the thermodynamic preference for **1** in the presence of acetonitrile.

Reactions with Hydrogen Peroxide. Addition of excess H₂O₂ to a solution of **1** in acetone or methanol resulted in the appearance of a deep purple color ($\lambda_{\text{max}} = 530 \text{ nm}$, $\epsilon = 1100 \text{ M}^{-1} \text{ cm}^{-1}$ or $\lambda_{\text{max}} = 548 \text{ nm}$, $\epsilon = 1100 \text{ M}^{-1} \text{ cm}^{-1}$, respectively)

- (27) Jonas, R. T.; Stack, T. D. P. *J. Am. Chem. Soc.* **1997**, *119*, 8566–8567.
 (28) Holman, T. R.; Andersen, K. A.; Anderson, O. P.; Hendrich, M. O.; Juarez-Garcia, C.; Münck, E.; Quel, L., Jr. *Angew. Chem., Int. Ed. Engl.* **1990**, *29*, 921–923.
 (29) Lecomte, C.; Chadwick, D. L.; Coppens, P.; Stevens, E. D. *Inorg. Chem.* **1983**, *22*, 2982–2992.
 (30) Hatano, K.; Uno, T. *Bull. Chem. Soc. Jpn.* **1990**, *63*, 1825–1827.
 (31) Hoard, J. L.; Hamor, M. J.; Hamor, T. A.; Caughey, W. S. *J. Am. Chem. Soc.* **1965**, *87*, 2312–2319.
 (32) Johnson, M. R.; Seok, W. K.; Ma, W.; Slobodnick, C.; Wilcoxon, K. M.; Ibers, J. A. *J. Org. Chem.* **1996**, *61*, 3298–3303.
 (33) Belle, C.; Gautier-Luneau, I.; Pierre, J.-L.; Scheer, C.; Saint-Aman, E. *Inorg. Chem.* **1996**, *35*, 3706–3708.
 (34) Karia, R.; Willey, G. R.; Drew, M. G. B. *J. Chem. Soc., Dalton Trans.* **1986**, 2493–2495.
 (35) Jeske, P.; Haselhorst, G.; Weyhermüller, T.; Wieghardt, K.; Nuber, B. *Inorg. Chem.* **1994**, *33*, 2462–2471.

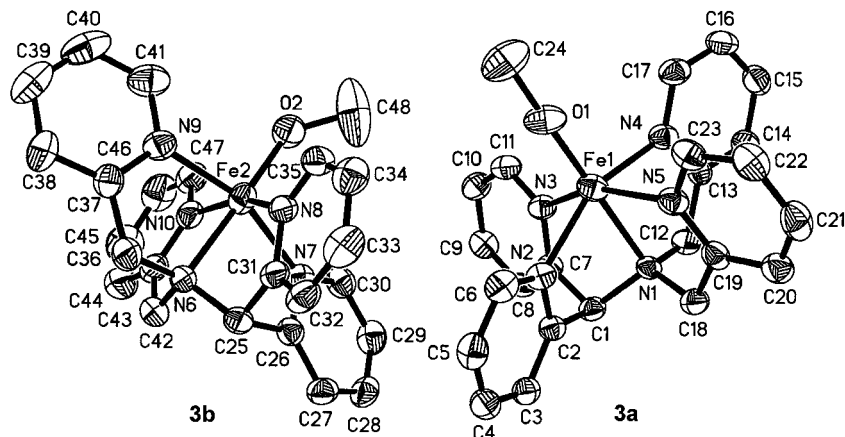


Figure 4. ORTEP plots of $[(\text{N4Py})\text{FeOMe}]^{2+}$ (**3**). Hydrogen atoms omitted for clarity.

Table 3. Comparison of Bond Lengths and Bond Angles of Complexes with an Fe^{III} -Terminal Methoxy Bond^a

	$\text{Fe}-\text{O}_{\text{methoxy}}$ (Å)	$(\text{C}-\text{O})_{\text{methoxy}}$ (Å)	$\text{Fe}-\text{O}-\text{CH}_3$ (deg)
3a	1.772	1.418	171.5
3b	1.789	1.375	136.5
$[(\text{PY5})\text{FeOMe}]^{2+ b}$	1.782	1.375	164.9
$[(\text{bpm})\text{Cu}^{\text{II}}\text{Fe}^{\text{III}}(\text{O}_2\text{CCH}_3)\text{OMe}]^{2+ c}$	1.849	1.402	136.4
$[(\text{L})\text{Fe}_2(\mu\text{-OMe})\text{OMe}]^{+ d}$	1.830	1.373	136.7
$[(\text{TPP})\text{FeOMe}]^e$	1.816	1.393	129.1
$[(\text{meso-DME})\text{FeOMe}]^f$	1.842	1.367	125.9
$[(\text{OEP})\text{FeOMe}]^g$	1.843	1.415	125.5
$[(\text{capped-Por})\text{FeOMe}]^h$	1.851	1.371	127.1

^a bpm = 2,6-bis((bis(2-pyridylmethyl)amino)methyl)-4-methylphenolate; L = 2-(bis(2'-hydroxyphenyl)amino)methyl-6-(bis(2''-pyridylmethyl)amino)methyl-4-methylphenolate; meso-DME = mesoporphyrin-IX dimethyl ester dianion; capped-Por = 1,2,4,5-tetrahydroxybenzene-capped tetra(*o*-ethoxyphenyl)porphyrin dianion;³³ OEP = octaethylporphyrin dianion; PY5 = 2,6-bis-((2-pyridyl)methoxymethane)pyridine; TPP = tetraphenylporphyrin dianion. ^b Reference 27. ^c Reference 28. ^d Reference 33. ^e Reference 29. ^f Reference 31. ^g Reference 30. ^h Reference 32.

ascribed to the $[(\text{N4Py})\text{FeOOH}](\text{ClO}_4)_2$ intermediate (**6**) as previously reported.¹² EPR spectroscopy characterized this species as a low-spin Fe^{III} complex with *g* values at 2.17, 2.12, and 1.98, and its formulation as an iron(III) hydroperoxide complex is confirmed using electrospray mass spectrometry.¹² At 25 °C the purple color disappeared within 15 min but could be regenerated by adding more H_2O_2 , implying that H_2O_2 decomposition is catalytic with respect to **1**. However, the purple color could not be recovered fully (~80%), meaning that some deactivation of the N4Py iron complex takes place during H_2O_2 turnover.

In contrast, **6** could be formed only to a small extent in acetonitrile, presumably because of the unfavorable equilibrium for displacing the acetonitrile ligand in **1**. Similarly the Fe^{III} -OOH intermediate could not be detected when H_2O_2 was added to **2**. This result may be a consequence of the axially coordinated chloride ligand, which cannot be as readily displaced by H_2O_2 so that the formation rate for intermediate **6** is not significantly faster than its decay rate. This observation corresponds with the results found for the reaction of $[(\text{TPA})_2\text{Fe}_2\text{O}(\text{H}_2\text{O}_2)](\text{CF}_3\text{SO}_3)_2$ ³⁶ and $[(\text{TPA})\text{FeCl}_2](\text{ClO}_4)$ with ^tBuOOH²⁴ in which an Fe^{III} -OO^tBu intermediate could be detected in the first case, but not in the second.

To gain insight into the mechanism of formation for the Fe^{III} -OOH intermediate, the starting Fe^{II} complex **1** was titrated with a 10 M H_2O_2 solution in acetone at room temperature and the spectral changes were monitored with UV/vis spectroscopy (Figure 5). Addition of up to 0.5 equiv of H_2O_2 caused the characteristic absorption of the starting complex at 458 nm to disappear, but the purple species did not form until more H_2O_2

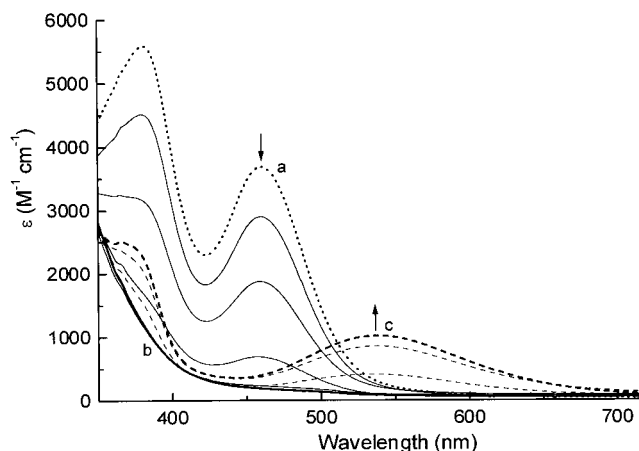


Figure 5. UV/vis titration of H_2O_2 to **1** in acetone at room temperature. (a) Dark dotted line: without H_2O_2 . (b) Dark solid line: with 0.5 equiv of H_2O_2 . (c) Dark dashed line: with 300 equiv of H_2O_2 . The light solid lines between a and b correspond to addition of 0.1–0.4 equiv of H_2O_2 . The light dashed lines between b and c correspond to the addition of 10 or 100 equiv of H_2O_2 .

was added. These results indicate that the Fe^{III} -OOH intermediate **6** is formed in a two-step process (Scheme 2). The products formed after addition of 0.5 equiv of H_2O_2 could be precipitated by adding excess diethyl ether. The ¹H NMR spectrum of the precipitate in CD_3CN (Figure 6) revealed the presence of two paramagnetic species. The signals in the 0–40 ppm range are characteristic for an antiferromagnetically coupled (μ -oxo)diiron(III) dimer, identified as **4**. The signals at –10 to 0 ppm and 80 to 120 ppm are indicative of a mononuclear high-spin Fe^{III} species and resemble those of **3**; this second complex is thus tentatively characterized as $[(\text{N4Py})\text{FeOH}](\text{ClO}_4)_2$ (**5**). Further

(36) Kim, J.; Larka, E.; Wilkinson, E. C.; Que, L., Jr. *Angew. Chem., Int. Ed. Engl.* **1995**, *34*, 2048–2051.

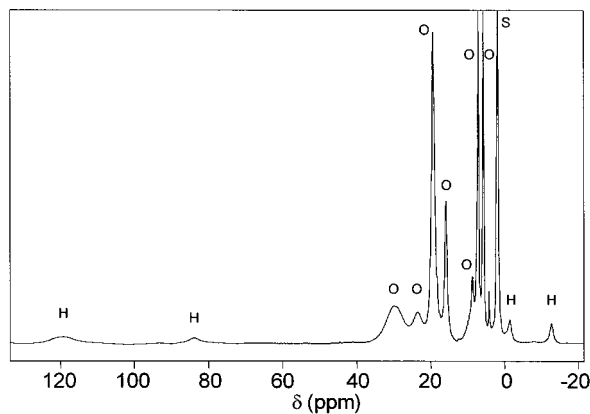
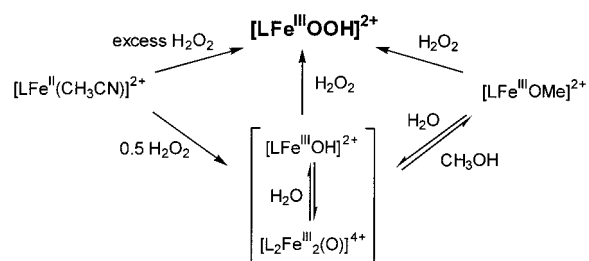


Figure 6. ^1H NMR spectra of the reaction mixture in CD_3CN after addition of 0.5 equiv of H_2O_2 to **1**, showing the signals of $[(\text{N}4\text{Py})\text{FeOH}]^{2+}$ (H), $[(\text{N}4\text{Py})_2\text{Fe}_2\text{O}]^{4+}$ (O), and solvent (S).

Scheme 2. Formation of the $[(\text{N}4\text{Py})\text{FeOOH}]^{2+}$ Intermediate **6** from **1** and H_2O_2



reaction with H_2O_2 then gives the $[(\text{N}4\text{Py})\text{FeOOH}]^{2+}$ intermediate.

Solutions of **3** or **4** in acetone or methanol treated with 1 equiv H_2O_2 at -20°C per iron atom also show the intense purple color (λ_{max} at 530 nm in acetone and 548 nm in methanol) characteristic of the $\text{Fe}^{\text{III}}\text{—OOH}$ intermediate **6**. The extinction coefficients found are comparable to what is seen in the reaction of **1** with H_2O_2 . These experiments clearly demonstrate that both the $[(\text{N}4\text{Py})_2\text{Fe}_2\text{O}]^{4+}$ and the $[(\text{N}4\text{Py})\text{FeOMe}]^{2+}$ complexes (and presumably the $[(\text{N}4\text{Py})\text{FeOH}]^{2+}$ complex as well) can be converted to the $[(\text{N}4\text{Py})\text{FeOOH}]^{2+}$ intermediate **6** by simple acid–base chemistry. The facile equilibrium between **4** and **5** is in sharp contrast with heme iron chemistry where the FeOFe species is strongly favored.³⁷

Laser excitation into the 530 nm absorption band of **6** in acetone at 77 K gives the resonance Raman spectrum shown in Figure 7A, with four enhanced features at 632, 651, 672, and 790 cm^{-1} . The same characteristic Raman features are observed using the different starting compounds and different solvents, confirming that the same intermediate is being generated in all the H_2O_2 reactions. Intermediate **6** represents the first low-spin mononuclear iron hydroperoxide species to be characterized by resonance Raman spectroscopy.³⁸ The use of $\text{H}_2^{18}\text{O}_2$ (Figure 7B) causes only the features at 632 and 790 cm^{-1} to shift, to 616 and 746 cm^{-1} , respectively. The downshift by -44 cm^{-1} for the 790 cm^{-1} feature is close to the value of -45 cm^{-1} predicted by Hooke's Law for a pure O–O stretch, leading to its assignment as $\nu(\text{O}=\text{O})$. However, the downshift of the 632 cm^{-1} feature by only -16 cm^{-1} is significantly lower than predicted for a pure Fe–O vibration (-28 cm^{-1}). Inclusion of the other peroxo oxygen, i.e., $\nu(\text{Fe}=\text{OO})$, in the calculations

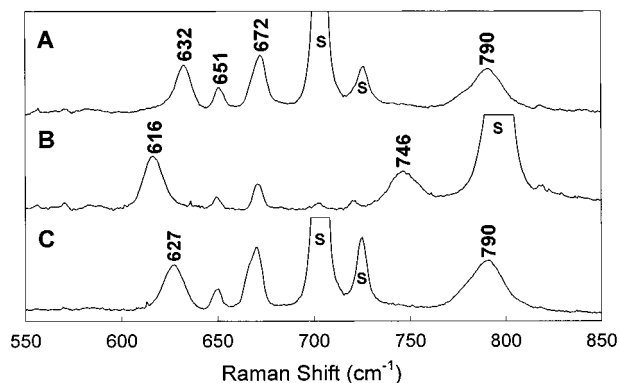


Figure 7. Resonance Raman spectra of **6**. (A) H_2O_2 (50 mM) was added to 10 mM $[\text{Fe}^{\text{II}}(\text{N}4\text{Py})(\text{CH}_3\text{CN})]^{2+}$ in d_6 -acetone at -10°C . The spectrum was obtained with 615 nm laser excitation at 20 mW power at the sample. (B) Same as A, except $\text{H}_2^{18}\text{O}_2$ and acetone were used. (C) Same as A, except H_2O_2 diluted in D_2O was used.

affords a downshift (-23 cm^{-1}) that approaches the experimental value, and the further addition of a proton, i.e., $\nu(\text{Fe}=\text{OOH})$, makes the downshift (-22 cm^{-1}) even closer. Support for the involvement of the hydroperoxy group in the 632 cm^{-1} deformation comes from the -5 cm^{-1} downshift observed upon ^2H labeling (Figure 7C), close to the calculated shift of -6 cm^{-1} for a $\nu(\text{Fe}=\text{OOH})$. Thus the ^{18}O and ^2H effects on the 632 cm^{-1} feature suggest that this feature arises from a coupled mode of the Fe–OOH unit.

The Raman features at 790 and 632 cm^{-1} associated with **6** are distinct from other iron–peroxo species which in general have $\nu(\text{O}=\text{O})$'s at 806–900 cm^{-1} and $\nu(\text{Fe}=\text{O})$'s at 421–503 cm^{-1} (Table 4).^{39–41} Most of these are (μ -1,2-peroxo)diron(III) species, so the most salient comparisons are with oxyhemerythrin (844, 503 cm^{-1})⁴⁰ and $[\text{Fe}^{\text{III}}(\text{EDTA})(\eta^2\text{-O}_2)]^{3-}$ (816, 459 cm^{-1}),³⁹ which are the only complexes with terminally bound peroxide characterized by resonance Raman spectroscopy. Oxyhemerythrin, like **6**, has a terminal hydroperoxide ligand, but $[\text{Fe}^{\text{III}}(\text{EDTA})(\eta^2\text{-O}_2)]^{3-}$ has a side-on bound peroxide. The most dramatic difference among these three iron peroxo species is observed for the lower frequency vibration, which for **6** is at least 129 cm^{-1} higher than the corresponding vibrations in the other two complexes. The significantly higher energy of this vibration in **6** may arise from the presence of a low-spin Fe^{III} center in **6**, the other two complexes having high-spin Fe^{III} centers. Furthermore, recent calculations using nonlocal density functional theory on the putative low-spin $\text{Fe}^{\text{III}}\text{—OOH}$ intermediate in cytochrome P450 suggest that the protonation of the

(37) Momenteau, M.; Reed, C. A. *Chem. Rev.* **1994**, *94*, 659–698.

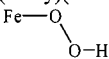
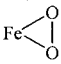
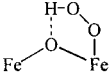
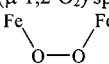
(38) Ho, R. Y. N.; Roelfs, G.; Feringa, B. L.; Que, L., Jr. *J. Am. Chem. Soc.* **1999**, *121*, 264–265.

(39) (a) Neese, F.; Solomon, E. I. *J. Am. Chem. Soc.* **1998**, *120*, 12829–12848. (b) Ahmad, S.; McCallum, J. D.; Shiemke, A. K.; Appelman, E. H.; Loehr, T. M.; Sanders-Loehr, J. *Inorg. Chem.* **1988**, *27*, 2230–2233.

(40) (a) Kurtz, D. M., Jr.; Shriver, D. F.; Klotz, I. M. *J. Am. Chem. Soc.* **1976**, *98*, 5033. (b) Shiemke, A. K.; Loehr, T. M.; Sanders-Loehr, J. *J. Am. Chem. Soc.* **1984**, *106*, 4951–4956.

(41) (a) Murch, B. P.; Bradley, F. C.; Que, L., Jr. *J. Am. Chem. Soc.* **1986**, *108*, 5027–5028. (b) Kitajima, N.; Fukui, H.; Moro-oka, Y.; Mizutani, Y.; Kitagawa, T. *J. Am. Chem. Soc.* **1990**, *112*, 6402–6403. (c) Brennan, B. A.; Chen, Q.; Juarez-Garcia, C.; True, A. E.; O'Connor, C. J.; Que, L., Jr. *Inorg. Chem.* **1991**, *30*, 1937–1943. (d) Kitajima, N.; Tamura, N.; Tanaka, M.; Moro-oka, Y. *Inorg. Chem.* **1992**, *31*, 3342–3343. (e) Dong, Y.; Ménage, S.; Brennan, B. A.; Elgren, T. E.; Jang, H. G.; Pearce, L. L.; Que, L., Jr. *J. Am. Chem. Soc.* **1993**, *115*, 1851–1859. (f) Kim, K.; Lippard, S. J. *J. Am. Chem. Soc.* **1996**, *118*, 4914–4915. (g) Dong, Y.; Zang, Y.; Kauffmann, K.; Shu, L.; Wilkinson, E. C.; Münck, E.; Que, L., Jr. *J. Am. Chem. Soc.* **1997**, *119*, 12683–12684. (h) Moënné-Loccoz, P.; Baldwin, J.; Ley, B. A.; Loehr, T. M.; Bollinger, J. M., Jr. *Biochemistry* **1998**, *37*, 14659–14663. (i) Broadwater, J. A.; Ai, J.; Loehr, T. M.; Sanders-Loehr, J.; Fox, B. G. *Biochemistry* **1998**, *37*, 14664–14671.

Table 4. Comparison of Resonance Raman Vibrations for Iron–Peroxide Complexes

Complex/Peroxide Binding Mode	$\nu_{\text{Fe-L}}$ (cm ⁻¹) ^a	$\nu_{\text{O-O}}$ (cm ⁻¹)	ref
[Fe(N4Py)(OOH)] ²⁺ 	632 ^b	790	38
[Fe(III)(EDTA)(η ² -O ₂)] ³⁻ 	459	816	39
oxyhemerythrin 	503	844	40
Fe ₂ (μ-1,2-O ₂) species 	415-476	848-900	41

^a L = O or OOH. ^b Observed feature for the coupled Fe–OOH mode.

Fe^{III}–OO⁻ intermediate results in the strengthening of the Fe–O bond and the weakening of the O–O bond.⁴² This proposed effect of protonation is entirely consistent with the high energy observed for the coupled Fe–OOH vibration in **6** and the fact that **6** has the lowest reported $\nu(\text{O–O})$ of all the Fe–peroxide complexes. Therefore the distinctive Raman features observed in **6** may serve as the Raman signature for a low-spin iron(III)–hydroperoxide intermediate.

The chemistry of the (N4Py)Fe^{III} center closely resembles that of (BLM)Fe^{III}, particularly with respect to the formation

of a low-spin Fe^{III}–OOH intermediate, which corresponds to activated bleomycin, the active form of the drug.⁸ Like bleomycin, N4Py is a pentadentate N5 ligand that forms well-defined Fe^{II} and Fe^{III} complexes. Although N4Py does not reproduce the coordination environment of BLM as closely as PMA¹⁰ and PYML,¹¹ a correspondence in the EPR spectra is observed. The metal centers in BLM and N4Py give rise to OH complexes with similarly rhombic EPR signals ($g = 2.43, 2.19, 1.89$ and $g = 2.41, 2.15, 1.92$ for BLM²⁰ and N4Py, respectively), and both decrease in rhombicity when the apical OH is replaced by OOH ($g = 2.26, 2.17, 1.94$ and $g = 2.19, 2.14, 1.97$ for BLM²⁰ and N4Py, respectively). More importantly the greater stability of the low-spin iron(III)–hydroperoxide intermediate of N4Py has allowed a more complete spectroscopic characterization of such species. Particularly interesting is the Raman spectrum of **6**, which shows a weakening of the O–O bond compared to all other iron–peroxo complexes that have been studied. This weakened O–O bond correlates well with the high reactivity proposed for low-spin iron(III)–hydroperoxide species. Further spectroscopic and reactivity studies on this intermediate should provide more information about the mechanism of action of Fe(III)–OOH species that occur in Nature as well as in oxidation catalysis.

Acknowledgment. This work was supported by the Unilever Research Laboratory, Vlaardingen, The Netherlands, and the National Institutes of Health (Grant GM-33162). R.Y.N.H. acknowledges an NIH postdoctoral fellowship (GM-17849).

Supporting Information Available: Three X-ray crystallographic files for **1**, **3**, and **4** in CIF format. This material is available free of charge via the Internet at <http://pubs.acs.org>.

(42) Harris, D. L.; Loew, G. H. *J. Am. Chem. Soc.* **1998**, *120*, 8941–8948.